



TITLE:

Optimized synthesis method for K/Co₃O₄ catalyst towards direct decomposition of N₂O

AUTHOR(S):

Yoshino, Hiroaki; Ohnishi, Chie H.; Hosokawa, Saburo; Wada, Kenji; Inoue, Masashi

CITATION:

Yoshino, Hiroaki ...[et al]. Optimized synthesis method for K/Co₃O₄ catalyst towards direct decomposition of N₂O. Journal of Materials Science 2011, 46(3): 797-805

ISSUE DATE:

2011-02

URL:

<http://hdl.handle.net/2433/137412>

RIGHT:

The final publication is available at www.springerlink.com; This is not the published version. Please cite only the published version.; この論文は出版社版ではありません。引用の際には出版社版をご確認ご利用ください。

Optimized synthesis method for $\text{K/Co}_3\text{O}_4$ catalyst towards direct decomposition of N_2O

Hiroaki Yoshino · Chie H. Ohnishi · Saburo Hosokawa · Kenji Wada ·

Masashi Inoue

Key words

Cobalt oxide, Catalyst synthesis, Nitrous oxide, Potassium promoter

H. Yoshino · C.H. Ohnishi · S. Hosokawa · K. Wada · M. Inoue (Corresponding
author)

Department of Energy and Hydrocarbon Chemistry, Graduate School of Engineering,

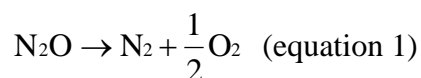
Kyoto University, Katsura, Kyoto 615-8510, Japan

e-mail: inoue@scl.kyoto-u.ac.jp

Abstract The potassium-doped Co_3O_4 catalysts were prepared by impregnation of potassium sources on commercial cobalt carbonate and on the precursors synthesized by homogeneous precipitation, combustion with glycine, gradual oxidation, and hydrothermal methods. The activities of these catalysts for the direct decomposition of nitrous oxide in the presence of oxygen with or without water vapor were examined. The effects of potassium sources on the catalyst activity were also examined by impregnation of various potassium salts on commercial cobalt carbonate. The catalyst prepared by impregnation of an aqueous solution of KOH on commercial cobalt carbonate showed the highest activity. The catalysts prepared by various methods were analyzed by powder X-ray diffraction, N_2 adsorption, scanning electron microscope, temperature-programmed reduction with H_2 , temperature-programmed desorption of O_2 , and X-ray photoelectron spectroscopy. These results suggest that crystallite size and reduction property are key factors for the activity of the catalyst for the direct decomposition of nitrous oxide in the presence of oxygen.

Introduction

Recently, catalytic removal of nitrous oxide (N₂O) from industrial exhaust has attracted much attention, because N₂O has been reported to have a significant global warming potential 310 times larger than that of CO₂ [1] and to contribute to the destruction of the ozone layer in the stratosphere [2]. So far, noble metals [2–6], metal oxides [7–11], and ion-exchanged zeolites [12–14] have been reported to exhibit catalytic activity towards the direct decomposition of nitrous oxide (eq. 1). Besides N₂O abatement from exhaust gases, catalytic decomposition of N₂O was also proposed as the propulsion system for small spacecrafts [15,16].



The significant anthropogenic sources of N₂O are nitric acid plants and adipic acid plants. However, the N₂O concentration in the tail gases from the adipic acid plants is relatively high (20–60%) [17], and thermal decomposition of N₂O [17,18] may be more economical because this method gives NO, besides N₂ and O₂, from which nitric acid, the oxidizing agent for the formation of adipic acid from the mixture of cyclohexanol and cyclohexanone, can be regenerated. For the tail gases from the nitric acid plants, catalytic decomposition seems to be a suitable solution [13, 19].

Excellent catalytic activities of cobalt oxides for N_2O abatement have been long recognized. Early works took notice of the activity of CoO [20–22]. However, its activity readily deteriorated because of the oxidation of the catalyst by N_2O [21].

Then, cobalt-based catalysts derived from hydrotalcites gathered much attention because spinel catalysts having large surface areas and high thermal stabilities can be easily prepared from the hydrotalcites obtained by co-precipitation methods [23–25]. Various catalyst systems prepared by this route have been proposed such as Co-Al [23, 24], Co-Mg [25,26], Co-Ni , [26], Co-Zn [27] and Co-Mn [28].

In patent literature, Armor *et al.* [29] claimed that the addition of Na^+ ions to the catalyst derived from a Co-Al hydrotalcite significantly increased the N_2O decomposition activity of the catalyst. Pérez-Ramírez *et al.* [30] noted that the deN_2O activity of a Co-Rh,Al catalyst was considerably affected by Na^+ ions remaining in the catalyst from the co-precipitation step for the synthesis of the hydrotalcite precursor. Unfortunately, this description has not drawn attention of the deN_2O researchers, because main theme of their paper is to propose the dual-bed system for NO_x removal from the flue gases from lean-burn engines.

We found that when precursors were prepared by precipitation of $\text{Co}(\text{NO}_3)_2$ with Na_2CO_3 and were thoroughly washed, the alkali content in the Co_3O_4 catalyst

depended on the crystal structure of the precursor, thus precipitation conditions affecting the catalyst activity [31]. The Co_3O_4 catalyst promoted by a proper amount of alkali ions is quite effective for the direct decomposition of N_2O in the presence of oxygen [32], maintaining its activity at least for 12 h in the presence of both oxygen and water. The addition of alkali ions to Co_3O_4 was found to promote the regeneration of Co^{2+} from Co^{3+} formed during N_2O decomposition [33]. Simultaneously, Xue *et al.* [34] reported the promotion effect of residual Na^+ ion on the activity of Co-Ce catalyst prepared by co-precipitation using K_2CO_3 as a precipitant. Since then, many papers have reported excellent promoting effects of alkali or alkaline earth components on the de N_2O activity of cobalt-based catalysts [35–41]. Note that excellent activities of alkali-promoted Co_3O_4 catalysts for the direct decomposition of NO were also reported by Park *et al.* [42] and Haneda *et al.* [43].

As mentioned above, preparation method for the alkali-promoted Co_3O_4 catalyst significantly affects its activity for N_2O decomposition; however, such effects have not been systematically investigated so far. In the present study, therefore, we have optimized the preparation method for the potassium-doped Co_3O_4 catalyst by changing the precursors of Co_3O_4 and potassium sources to maximize the activity for the direct decomposition of nitrous oxide in the presence of oxygen and/or water vapor. The

results presented here clearly suggest that several key factors govern the activity of the catalyst.

Experimental section

Preparation of K-doped Co_3O_4 catalysts

Catalysts were prepared by: (a) impregnation of commercial cobalt(II) carbonate [32, 33], (b) homogeneous precipitation [44], (c) combustion with glycine [45], (d) gradual oxidation [46], and (e) hydrothermal synthesis [47]. The details are as follows.

(a) Impregnation of commercial cobalt(II) carbonate [32, 33]

Commercial cobalt(II) carbonate (Nacalai Tesque, 0.020 mol) was impregnated with an aqueous solution (2 cm^3) of KNO_3 (Wako, 4.0×10^{-4} mol; atomic ratio of K/Co, 0.02) on an 80 °C water bath, and the $\text{K/Co}_3\text{O}_4$ catalyst was obtained by the calcination of the dried powder at 400 °C for 4 h in air. The catalyst is designated as catalyst A.

For comparison, cobalt oxide, which was prepared by the calcination of commercial cobalt(II) carbonate at 400 °C in air for 4 h, was impregnated with an aqueous solution (2 cm³) of KNO₃ (4.0×10^{-4} mol; atomic ratio of K/Co, 0.02) at 80 °C followed by drying and calcination at 400 °C for 1 h in air to give catalyst **A'**.

(b) Homogeneous precipitation [44]

Cobalt nitrate hexahydrate (Co(NO₃)₃·6H₂O; Wako, 0.050 mol) and urea (Wako, 0.10 mol) were dissolved in deionized water (750 cm³). The mixture was heated in an oil bath. The bath temperature was increased from room temperature to 120 °C and kept at 120 °C for 2 h. After the mixture had been cooled, the resulting powder was washed with deionized water three times and with methanol once by centrifuging and then air-dried. The resulting precursor was impregnated with an aqueous KNO₃ solution (0.20 M; K/Co = 0.02), dried at 80 °C, and calcined at 400 °C in air for 4 h. This sample is called catalyst **B**.

(c) Combustion with glycine [45]

Cobalt nitrate hexahydrate, glycine (Nacalai Tesque) and KNO₃ were dissolved in a

small amount of deionized water. The glycine/Co molar ratio was 1.2, and K/Co molar ratio was 0.02. The mixed solution was heated on an electric hot plate kept at 300 °C. When vigorous reaction started, heating was stopped. The product was calcined at 400 °C for 4 h in air. This sample is designated as catalyst **C**.

(d) Gradual oxidation [46]

In a three-neck flask, NaOH (0.030 mol) and NaNO₃ (1.0 mol) were dissolved in deionized water (100 cm³), and 1.0 M aqueous Co(NO₃)₂ solution (20 cm³) was added gradually over a period of 45 s. The mixture was kept in a 95 °C oil bath for 42 h with bubbling of air (70 cm³ min⁻¹). After the mixture had been cooled, the resulting powder was washed with deionized water three times and with methanol once by centrifuging and then air-dried. The thus-obtained precursor was impregnated with a KNO₃ solution (K/Co = 0.02), dried, and calcined at 400 °C for 4 h as described above (catalyst **D**).

(e) Hydrothermal synthesis [47]

Cobalt chloride hexahydrate (CoCl₂·6H₂O; Wako, 0.019 mol) and urea (0.019 mol)

were dissolved in deionized water (190 cm³) and the solution was placed in a Teflon autoclave. Then, the autoclave was sealed and kept at 100 °C for 12 h. After the mixture had been cooled, the resulting powder was washed three times with deionized water and with methanol once by centrifuging and then air-dried. Following the method for preparation of catalyst **A**, the precursor was impregnated with an aqueous solution of KNO₃ (K/Co = 0.02) and calcined at 400 °C for 4 h (catalyst **E**).

Catalyst activity test

Catalyst tests were carried out in a fixed-bed flow reactor. The catalyst was tabletted, pulverized into 10–22 mesh, and set in the reactor. The catalyst bed was heated to 500 °C and held at that temperature for 30 min in a helium flow. Then, the reaction gas composed of 5000 ppm N₂O, 2.0% O₂, 0 or 2.5% H₂O, and He balance was introduced to the catalyst bed at $W/F = 0.30 \text{ g s cm}^{-3}$. The effluent gases from the reactor were analyzed every 5 min with an on-line micro gas-chromatograph (CP 2002, Chrompack, Netherlands) (columns: 10 m Molecular Sieve 5A at 80 °C; 10 m Porapack Q at 40 °C). After the steady state was attained, reaction temperature was decreased, and the catalyst performance was measured at every 50 °C from 500 °C to the temperature where N₂O

conversion was negligible.

Characterization of the catalysts

Powder X-ray diffraction (XRD) pattern was recorded on a Shimadzu XD-D1 diffractometer using Cu *Ka* radiation through a carbon monochromator. The crystallite size of Co₃O₄ was calculated from the full width at half maximum (FWHM) of the diffraction peak at around 65° (2θ) using Scherrer equation:

$$D(\text{nm}) = \frac{0.9 \times 0.1542}{\beta \times \cos \theta}$$

where D is the crystallite size; θ , the diffraction angle; and $\beta = \beta_{\text{exp}} - \beta_{\text{app}}$. Here, β_{exp} and β_{app} are the FWHM of the diffraction peak and the instrumental broadening width, respectively. The specific surface area was calculated using the BET single-point method from nitrogen uptake measured at 77 K by using a Micromeritics FlowSorb II 2300 sorption-meter. The samples were pretreated in a N₂ flow at 300 °C for 30 min prior to the measurements. The apparent shape and size of the catalyst particles were observed using a Hitachi S-2500 CX scanning electron microscope (SEM). The

catalysts were also characterized by temperature-programmed reduction with H_2 (H_2 -TPR). A portion (0.010 g) of a sample was set in a reactor, activated at 500 °C for 1 h in an Ar flow and cooled to room temperature. Hydrogen (2 vol% H_2 -Ar; 20 cm³ min⁻¹) was introduced to the reactor and the sample was heated at a rate of 5 °C min⁻¹ up to 600 °C. The hydrogen content in the effluent gas from the reactor was measured by a TCD detector of a Shimadzu GC-8A gas chromatograph. Temperature-programmed desorption (TPD) of O_2 was also carried out in the fixed-bed flow reactor. The pretreatment conditions were the same as in the case of the catalyst tests (500 °C, 30 min in He). After the heat treatment in the helium flow, the temperature of the catalyst bed was decreased to 50 °C. The sample was kept at 50 °C in a flow of gas composed of 2% O_2 with helium balance ($W/F = 0.3 \text{ g s cm}^{-3}$) for 1 h, and then purged with He (100 cm³ min⁻¹) for 1 h. After the treatment, the temperature was raised to 500 °C at a rate of 5 °C min⁻¹ in the helium flow, and the effluent gas from the reactor was continuously analyzed with a Pfeiffer Vacuum Omnistar GSD 301 O 1 quadrupole mass spectrometer. The XPS measurements were carried out with an ULVAC-PHI model 5500 spectrometer with Mg $K\alpha$ emission (15 kV, 400 W) as the X-ray source. The binding energy was corrected by the contaminated carbon (284.6 eV) [48].

Results and discussion

Effects of the preparation methods on the properties of the catalysts

In order to examine effect of the preparation method on the activity for N_2O decomposition, six K-doped Co_3O_4 catalysts were prepared by various methods described in Experimental Section. The homogeneous precipitation method via urea hydrolysis has been applied for the preparation of various materials. It was reported that the BET surface areas of $\text{CeO}_2\text{-ZrO}_2$ catalysts prepared by this method are reasonably large [44]. $\text{Lu}_{1.98}\text{Ln}_{0.02}\text{O}_3$ ($\text{Ln} = \text{Nd, Eu, and Er}$) powders obtained by propellant synthesis via combustion with glycine were reported to have a very porous, open morphology [45]. Free-standing Co_3O_4 nanocubes with a uniform size of *ca.* 47 nm have been prepared by the gradual oxidation method [46]. The Co_3O_4 nanorods with a porous structure were obtained through the thermal treatment of $\text{Co}(\text{CO}_3)_{0.35}\text{Cl}_{0.20}(\text{OH})_{1.10}$ prepared by hydrothermal reaction of CoCl_2 with urea [47].

The catalysts were characterized by XRD, SEM, H_2 -TPR, O_2 -TPD, nitrogen adsorption/desorption, and XPS to investigate the effects of the preparation methods on

the properties of the catalysts. Figure 1 shows the XRD patterns of the precursors of the K/Co₃O₄ catalysts, and the phases detected by XRD are summarized in Table 1. The XRD pattern of the precursor obtained by the homogeneous precipitation method (catalyst **B**) was assigned to a hydrotalcite-like phase [49]. The XRD study also revealed that a mixture of the crystalline Co₃O₄ and CoO was obtained by the combustion method (JCPDS Cards No. 9-418 and 9-402, respectively) (catalyst **C**), while hydrothermal reaction of CoCl₂ with urea yielded Co(CO₃)_{0.35}Cl_{0.20}(OH)_{1.10} (JCPDS Card No. 38-547) (catalyst **E**). The XRD pattern of the precursor obtained by gradual oxidation method (catalyst **D**) is attributed to crystalline Co₃O₄, Co(OH)₂(NO₃)_x · nH₂O and Co(OH)_{2-x}(NO₃)_x · nH₂O phases [46].

Figure 2 shows the XRD patterns of K-doped Co₃O₄ catalysts after the calcination. All the XRD peaks are due to crystalline Co₃O₄. As shown in Table 2, crystallite size of the Co₃O₄ phase of catalysts **A**, **B** and **C** were relatively small, whereas those of catalysts **D** and **E** were significantly large. Because the temperature at which the catalysts were pretreated prior to the catalytic runs is higher than the calcination temperature of the samples characterized, data for both the fresh and spent catalysts are given in Table 2. Although the BET surface area of each catalyst decreased by the pretreatment (Table 2), it was significantly affected by the preparation method,

and decreased in the following order; catalyst **A** > **B** > **D** > **E** > **C**. Catalyst **C** had a surface area much smaller than that expected from the crystallite size, indicating that the primary particles were severely aggregated.

The extent of the aggregation of primary particles is obvious through the SEM observation as well (Fig. 3). Whereas catalyst **C** had large pores, the surface of the particles was very smooth, indicating severe aggregation of primary particles, in consistent with the discussion mentioned above. Catalyst **E** was composed of nanorods with smooth surface. Catalysts **B** and **D** were comprised of small particles. On the other hand, the catalyst **A** was composed of large spherical aggregates of fine particles.

The results for XPS data are summarized in Table 3. All the catalysts exhibited the peak due to Co 2p_{3/2} at binding energy of 779.6–780.1 eV, which was in reasonable agreement with the reported data (779.8 eV) for Co₃O₄ [50, 51]. It is rather surprising to know that the K/Co ratios in the surface region of catalysts **A** and **C** were rather high in spite of the fact that the former catalyst had a relatively large surface area. This result seems to connect with the morphology of the precursor particles which were essentially identical with the morphology of the catalysts (Fig. 3). Since we impregnated the precursors with a KNO₃ solution, the promoter is enriched on the outer surface of the particles, and large precursor particles such as CoCO₃ gave high K/Co ratios because

the XPS analysis also gives the data for the composition at the surface region of the aggregated particles

The effects of preparation methods on the reduction behavior of the K-doped Co_3O_4 catalysts were investigated by the H_2 -TPR technique (Fig. 4). For catalyst **A**, two reduction peaks were observed at around 200 °C and 250–400 °C. The former peak is attributed to the reduction of Co^{3+} to Co^{2+} , while the latter is due to the reduction of Co^{2+} to Co metal [33, 35, 52, 53]. The hydrogen consumption at <200 °C, as indicated by shadow in Fig. 4, was much significant for catalyst **A**, less pronounced for catalysts **B** and **C**. On the other hand, catalysts **D** and **E** did not show distinct hydrogen consumption in this temperature range, suggesting that the reduction of Co^{3+} to Co^{2+} might occur at higher temperatures. In previous studies [33, 35], a good correlation was found between the N_2O decomposition activity of the catalysts and the intensity of the peak at around 200 °C in the TPR profiles, and the promotion of the regeneration of the Co^{2+} species in the catalytic cycle at lower temperatures was proposed to be responsible for the enhanced catalyst activity. The present results clearly indicate that preparation methods of the catalysts significantly affect the extent of the reduction of Co^{3+} to Co^{2+} at lower temperatures.

Figure 5 shows the O_2 -TPD profiles of the K/ Co_3O_4 catalysts prepared by

various methods. The desorption peaks were observed at 50–180 °C and above 400 °C. The former and latter peaks are assigned to the desorption of adsorbed oxygen and elimination of lattice oxygen, respectively [33]. Catalysts **A**, **B**, **C**, and **D** showed an oxygen desorption peak at <180 °C. Meanwhile, the intensity of this peak decreased in the order **A** > **B** > **C** > **D**. On the other hand, catalyst **E** did not show any peak at such temperature range. Previous study [33] suggested that the number of oxygen adsorption sites correlates with the activity of the catalyst: The catalyst with higher activity for N₂O decomposition adsorbs a larger amount of oxygen exhibiting a large desorption peak at <180 °C. For the active catalysts, the deactivation caused by irreversible adsorption of oxygen on the catalyst surface [3, 5, 33] would be suppressed even in the presence of molecular oxygen.

Based on these results, the catalysts prepared in the present study can be classified into two categories: Catalysts **A**, **B** and **C** belong to the first category. These catalysts exhibited significant hydrogen consumption at <200 °C in H₂-TPR profiles and adsorbed large amounts of molecular oxygen. Catalysts **D** and **E** belong to the second category. These catalysts did not exhibit hydrogen consumption at <200 °C and adsorbed small or negligible amounts of molecular oxygen. The crystallite sizes of the catalysts in the first category were relatively small, while those of the catalysts in the

second category were much larger.

Effects of potassium sources on the reduction behavior of the K-doped Co_3O_4 catalyst were examined. Figure 6 shows the H_2 -TPR profiles of the catalysts prepared by impregnation of commercial cobalt(II) carbonate with various K salts followed by the calcination at 400 °C for 4 h. Again, there were two reduction peaks at around 200 °C and 250–400 °C, and the former peak was significant for the catalysts prepared using (a) KOH, (b) KNO_3 , (c) KHCO_3 , and (d) CH_3COOK , while the catalysts prepared using (e) K_2SO_4 and (f) KCl exhibited the peak at ~230 °C. Since unpromoted Co_3O_4 showed the peak at ~220 °C, thermally stable K precursors may have negative effect on reduction of the Co_3O_4 catalyst.

Effects of the preparation methods on the catalytic activity of $\text{K}/\text{Co}_3\text{O}_4$ for N_2O decomposition

The N_2O decomposition activities of the K-doped Co_3O_4 catalysts were compared under the dry conditions and the results are shown in Fig. 7. The catalytic activity decreased according to the following order: catalyst **A** \approx **A'** > **B** > **C** > **D** >> **E**. Such activity order matches well with the information abstracted from Fig. 5. For catalysts **A** and **A'**, N_2O

conversion to N_2 at 200 °C was >80 %. These results indicate that the order of the impregnation of KNO_3 and the decomposition of cobalt(II) carbonate does not affect the catalytic activity. On the other hand, catalyst **E** had an extremely low activity, and N_2O conversion was <10 % even at 500 °C. In this respect, XPS study revealed that a significant amount of Cl^- ($Cl/Co = 0.071$) was remaining on the surface of catalyst **E** (Table 3).

The catalytic activities for N_2O decomposition were markedly influenced by water present in the feed as shown in Fig. 8. This result suggests that water molecules adsorbed on the active sites hamper the N_2O decomposition. However, the order of activity of the catalysts under the wet conditions was the same as that found under the dry conditions. In Fig. 8, the data for catalyst **E** is not given because it did not exhibit a measurable N_2O decomposition activity even at 500 °C. Catalyst **A** showed the highest activity among the catalysts examined in this study and the activity of this catalyst was maintained at least for 12 h even in the presence of oxygen and water in the feed.

The effect of the K sources on the activities of the catalysts prepared by the impregnation of cobalt(II) carbonate followed by calcination was examined. Figure 9 shows that the results of the reactions under the dry conditions. The catalytic activity decreased according to the following order: $KOH > KNO_3 \approx KHCO_3 > CH_3OOK > >$

$\text{K}_2\text{SO}_4 > \text{KCl}$. Under the wet conditions, their activities again markedly decreased as shown in Fig. 10. However, the order of the activity was basically unchanged, and the differences in the activities between the catalysts modified with KOH, KNO_3 , KHCO_3 , and CH_3COOK were negligible. On the other hand, the catalysts prepared by using K_2SO_4 and KCl showed low activities. The presence of sulfates (0.6 atomic %) and Cl^- ions (2 atomic %) in the surface region of the catalyst particles was confirmed by XPS analysis. It is interesting to note that the activities of K_2SO_4 - and KCl-modified catalysts were higher than that of the unpromoted Co_3O_4 catalyst. This result indicates that K^+ ions derived from the hardly decomposable salts also have the promoting effect on the Co_3O_4 catalyst to some extent.

The combined results of the characterization and catalytic runs clearly show the close correlation between the redox behavior and the activity of the catalysts. The catalyst having easily reducible Co^{3+} species which adsorbed a large amount of molecular oxygen (exhibited an intense desorption peak at $<180^\circ\text{C}$ in the O_2 -TPD profile) showed an excellent activity for N_2O decomposition. On the contrary, the catalyst having only hardly-reducible Co^{3+} species showed a low activity. Possible reason for extremely poor activity of catalyst **E** would be Cl^- ion remaining on the surface of the catalyst. Note that the crystallite sizes of the active catalysts were

relatively small (see above). A large number of surface defects such as steps and kinks were exposed on the surface of the crystallites with smaller sizes. Recently, Xu *et al.* [54] studied the reaction mechanisms for catalytic oxidation of CO by N₂O on Co₃O₄(110) surfaces by DFT slab calculations, and found that N₂O reacts with the oxygen vacancy on the defect Co₃O₄(110) surface yielding N₂ and perfect Co₃O₄(110) surface. The reactions of N₂O with the surface oxygen vacancies are well known [55–59]. For example, Henderson *et al.* [57] found that oxygen vacancies on TiO₂(110), formed by annealing TiO₂(110) surface in vacuum at >800 K, react with N₂O even at 90 K resulting in ejection of N₂ and vacancy oxidation. However, such a process is not always catalytic, and Xu *et al.* [54] found that interaction between N₂O and perfect Co₃O₄(110) surface is quite weak, whereas oxygen vacancy is regenerated by the reaction of perfect Co₃O₄(110) surface with CO, a strong reducing agent. In the present study, such a reducing agent is absent, and therefore, the reaction of N₂O with oxygen vacancies is not involved in the catalytic cycle of the present catalyst system. Instead, we believe that surface defects such as steps and kinks act as the N₂O adsorption sites, where heat of adsorption of N₂O would be much smaller than that evolved when N₂O is adsorbed on oxygen vacancies. However, surface defects would be easily regenerated by desorption of O₂, which permit the catalytic cycle for N₂O decomposition. Since the

adsorption of atomic oxygen on the defect site is accompanied with the oxidation of Co^{2+} located in the defect, such Co^{2+} ions can be considered as the active sites for the N_2O decomposition through the redox mechanism [33, 36, 38, 40, 60–64].

The K^+ species on the catalysts were proposed to destabilize the oxygen atoms formed by the cleavage of N-O bond of N_2O , and thus promote desorption of oxygen molecules from the catalysts to regenerate the catalytically active species [33]. The results in the present study support this idea, but the effect of K-doping was found to be significantly influence by the counter anions. The use of K_2SO_4 and KCl was less effective. These results may be caused by sulfate and Cl^- ions remaining on the catalyst surface, because these anions are strongly adsorbed on the surface defects, thus hampering the N_2O decomposition reaction.

Conclusions

The activity of $\text{K}/\text{Co}_3\text{O}_4$ catalysts for the direct decomposition of nitrous oxide was greatly affected by both the preparation methods and potassium sources. Among the catalysts examined, the catalyst prepared by impregnation of CoCO_3 with an aqueous

solution of KOH showed the highest activity. The catalysts with smaller crystallite sizes generally showed higher activities. Chloride and sulfate ions remaining on the surface of the catalysts greatly inhibited their activities. The intensity of the O₂-desorption peak at <180 °C in O₂-TPD experiment was found to be a good diagnosis of the activity of the catalyst. The TPR measurements revealed that preparation methods of the catalysts as well as potassium sources significantly influenced the extent of the reduction of Co³⁺ to Co²⁺ at low temperature (~200 °C), which crucially affect the activity for N₂O decomposition.

References

1. Third Assessment Report of the IPCC, 2001
2. Kapteijn F, Rodriguez-Mirasol J, Moulijn J A (1996) *Appl Catal B: Environmental* 9:25–64
3. Centi G, Galli A, Montanari B, Perathoner S, Vaccari A (1997) *Catal Today* 35:113–120
4. Haber J, Machej T, Janas J, Nattich M (2004) *Catal Today* 90:15–19
5. Tzitzios VK, Georgakilas V (2005) *Chemosphere* 59:887–891
6. Haber J, Nattich M, Machej T (2008) *Appl Catal B: Environmental* 77: 278–283
7. Drago RS, Jurczyk K, Kob N (1997) *Appl Catal B: Environmental* 13:69–79
8. Satsuma A, Maeshima H, Watanabe K, Suzuki K, Hattori T (2000) *Catal Today* 63:347–353
9. Scagnelli A, di Valentin C, Pacchioni G (2006) *Surf Sci* 600:386–394
10. Russo N, Mescia D, Fino D, Saracco G, Specchia V (2007) *Ind Eng Chem Res* 46:4226–4231
11. Pasha N, Lingaiah, N, Reddy PSS, Prasad PSS, (2009) *Catal Lett* 127:101–106
12. da Cruz RS, Mascarenhas AJS, Andrade HMC (1998) *Appl Catal B: Environmental* 18:223–231

13. Pérez-Ramírez J, Kapteijn F, Mul G, Moulijn JA (2001) *Chem Commun* 693–694
14. Guesmi H, Berthomieu D, Kiwi-Minsker L (2008) *J Phys Chem C*
112:20319–20328
15. Zakirov V, Sweeting M, Lawtence T, Sellers J (2001) *Acta Astronaut* 48:353–362
16. Zakirov V, Zhang H-Y (2008) *Aerospace Sci Technol* 12:318–323
17. Shimizu A, Tanaka K, Fujimori M (2000) *Chemosphere Global Change Sci*
2:425–434
18. Shimizu A, Miura K, Tagawa K, Kan H (2004) *J Chem Eng Jpn* 37:808–813
19. Stelmachowski P, Zasada F, Maniak G, Granger P, Inger M, Wilk M, Kotarba A,
Sojka Z (2009) *Catal Lett* 130:637–641
20. Schmid G, Keller N (1950) *Naturwiss* 37:42–43
21. Amphlett CB (1954) *Trans Faraday Soc* 50:273–278
22. Volpe ML, Reddy JF (1967) *J Catal* 7:76–84
23. Armor JN, Braymer TA, Farris TS, Li Y, Petrocelli FP, Weist EL, Kannan S, Swamy
CS (1996) *Appl Catal B: Environmental* 7:397–406
24. Kannan S, Swamy CS (1999) *Catal Today* 53:725–737
25. Chellam U, Xu Z P, Zeng HC (2000) *Chem Mater* 12:650–658
26. Yan L, Ren T, Wang X, Ji D, Suo J (2003) *Appl Catal B: Environmental* 45:85–90

27. Yan L, Ren T, Wang X, Gao Q, Ji D, Suo J (2003) *Catal Commun* 4:505–509
28. Obalová L, Fíla (2007) *Appl Catal B: Environmental* 70:353–359
29. Armor JN, Braymer TA, Li Y, Farris TS (1995) USP 005472677 (Engelhard Co)
30. Pérez-Ramírez J, Garc  a-Cort  s JM, Kapteijn F, Ill  n-G  mez MJ, Ribera A, de Lecea CS-M, Moulijn JA (2000) *Appl Catal B: Environmental* 25:191–203
31. Ohnishi C, Asano K, Iwamoto S, Inoue M (2006) *Stud Surf Sci Catal* 162:737–744
32. Ohnishi C, Asano K, Iwamoto S, Chikama K, Inoue M (2007) *Catal Today* 120:145–150
33. Asano K, Ohnishi C, Iwamoto S, Shioya Y, Inoue M (2008) *Appl Catal B: Environmental* 78:242–249
34. Xue L, Zhang C, He H, Teraoka Y (2007) *Catal Today* 126:449–455
35. Pasha, N Lingaiah N, Babu NS, Reddy PSS, Presad PSS (2008) *Catal Commun* 10:132–136
36. Stelmachowski P, Maniak G, Kotarba A, Sojka Z (2009) *Catal Commun* 10:1062–1065
37. Zasada F, Stelmachowski P, Maniak G, Paul J-F, Kotarba A, Sojaka Z (2009) *Catal Lett* 127:1269–131
38. Abu-Zied BM, Soliman SA, (2009) *Catal Lett* 132: 299–310

39. Cheng H, Huang Y, Wang A, Li L, Wang X, Zhang T (2009) Appl Catal B: Environmental 89:391–397
40. Xue L, He H, Liu C, Zhang C, Zhang B (2009) Environ Sci Technol 43:890–895
41. Obalová L, Karásková K, Jiráťová K, Kovanda F (2009) Appl Catal B: Environmental 90:132–140
42. Park PW, Kil JK, Kung HH, Kung MC (1998) Catal Today 42:51–60
43. Haneda M, Kintaichi Y, Bion N, Hamada H (2003) Appl Catal B: Environmental 46:473–482
44. Pengpanich S, Meeyoo V, Rirksomboon T, Bunyakiat K (2002) Appl Catal A: General 234:221–233
45. Polizzi S, Bucella S, Speghini A, Vetrone F, Naccache R, Boyer JC, Capobianco JA (2004) Chem Mater 16:1330–1335
46. Xu R, Zeng HC (2003) J Phys Chem B 107:926–930
47. Wang Z, Chen X, Zhang M, Qian Y (2005) Solid State Sci 7:13–15
48. Moulder F, Stickle WF, Sobol PE, Bomben KD (1992) Handbook of X-Ray Photoelectron Spectroscopy, Perkin-Elmer Co, Eden Prairie (USA)
49. Xu R, Zeng HC (2003) J Phys Chem B 107:12643–12649
50. Haneda M, Nakamura I, Fujitani T, Hamada H (2006) Catal Survey Asia 9:207–215
51. Avila AG, Barrera EC, Huerta LA, Muhl A (2004) Solar Energy Mater Solar Cell

82:269–278

52. Sexton BA, Hughes AE, Turney TW (1986) *J Catal* 97:390–406

53. Voß M, Borgmann D, Wedler G (2002) *J Catal* 212:10–21

54. Xu, X-L; Yang, E; Li, J-Q, Li Y, Chen W-K (1991) *ChemCatChem* 1:384–392

55. Winter ERS (1969) *J Catal* 15:144–152

56. Cunningham J, Penny AL (1974) *J Phys Chem* 78 870–875

57. Henderson MA, Szanyi J, Peden CHF (2003) *Catal Today* 85:251–266

58. Zhu J, Albertsma S, van Ommen JG, Lefferts L (2005) *J Phys Chem B*
109:9550–9555

59. Chen W-K, Sun B-Z, Wang X, Lu C-H (2008) *J Theo Comput Chem* 7:263–276

60. Dandekar A, Vannice MA (1999) *Appl Catal B: Environmental* 22:179–200

61. Zhu Z, Lu GQ, Zhuang Y, Shen D (1999) *Energy Fuels* 13:763–772

62. Pinna F, Scarpa M, Strukul G, Guglielminotti E, Boccuzzi F, Manzoli M (2000) *J Catal* 192:158–162

63. Fanning PE, Vannice MA (2002) *J Catal* 207:166–182

64. Nobukawa T, Yoshida M, Okumura K, Tomishige K, Kunimori K (2005) *J Catal*
229:374–388

Figure captions

Fig. 1 XRD patterns of the precursors: (a), catalyst **A**; (b), catalyst **B**; (c), catalyst **C**; (d), catalyst **D**; (e), catalyst **E**.

Fig. 2 XRD patterns of K-doped Co_3O_4 catalysts: (a), catalyst **A**; (b), catalyst **B**; (c), catalyst **C**; (d), catalyst **D**; (e), catalyst **E**.

Fig. 3 SEM photographs of K-doped Co_3O_4 catalysts: (a), catalyst **A**; (b), catalyst **B**; (c), catalyst **C**; (d), catalyst **D**; (e), catalyst **E**.

Fig. 4 H_2 -TPR profiles of K-doped Co_3O_4 catalysts: (a), catalyst **A**; (b), catalyst **B**; (c), catalyst **C**; (d), catalyst **D**; (e), catalyst **E**.

Fig. 5 O_2 -TPD profiles of K-doped Co_3O_4 catalysts prepared by various methods.

Fig. 6 H_2 -TPR profiles of Co_3O_4 catalysts modified by: (a), KOH; (b), KNO_3 ; (c), KHCO_3 ; (d), CH_3COOK ; (e), K_2SO_4 ; (f), KCl; (g) unpromoted Co_3O_4 .

Fig. 7 N_2O decomposition activities of K/ Co_3O_4 catalysts: \blacklozenge , catalyst **A**; \blacktriangle , catalyst **A'**; \circ , catalyst **B**; \square , catalyst **C**; \blacktriangle , catalyst **D**; \times , catalyst **E**; under dry conditions. Reaction conditions: N_2O , 5,000 ppm; O_2 , 2 %; He balance; $W/F = 0.30 \text{ g s cm}^{-3}$.

Fig. 8 N_2O decomposition activities of K/ Co_3O_4 catalysts prepared by: \blacklozenge , catalyst **A**; \blacktriangle , catalyst **A'**; \circ , catalyst **B**; \square , catalyst **C**; \blacktriangle , catalyst **D**; under wet conditions. Reaction conditions: N_2O , 5,000 ppm; O_2 , 2 %; H_2O , 2.5 %; He balance; $W/F = 0.30 \text{ g s cm}^{-3}$.

Fig. 9 N₂O decomposition activities of Co₃O₄ catalysts modified by: ■, KOH; ◇, KNO₃; ○, KHCO₃; ×, CH₃COOK; ●, K₂SO₄; □, KCl; ▲, without K modification; under dry conditions. Reaction conditions: N₂O, 5,000 ppm; O₂, 2 %; He balance; $W/F = 0.30$ g s cm⁻³.

Fig. 10 N₂O decomposition activities of Co₃O₄ catalysts modified by: ■, KOH; ◇, KNO₃; ○, KHCO₃; ×, CH₃COOK; ●, K₂SO₄; □, KCl; ▲, without K modification; under wet conditions. Reaction conditions: N₂O, 5,000 ppm; O₂, 2 %; H₂O, 2.5 %; He balance; $W/F = 0.30$ g s cm⁻³.

Table 1 Precursor phase for XRD patterns

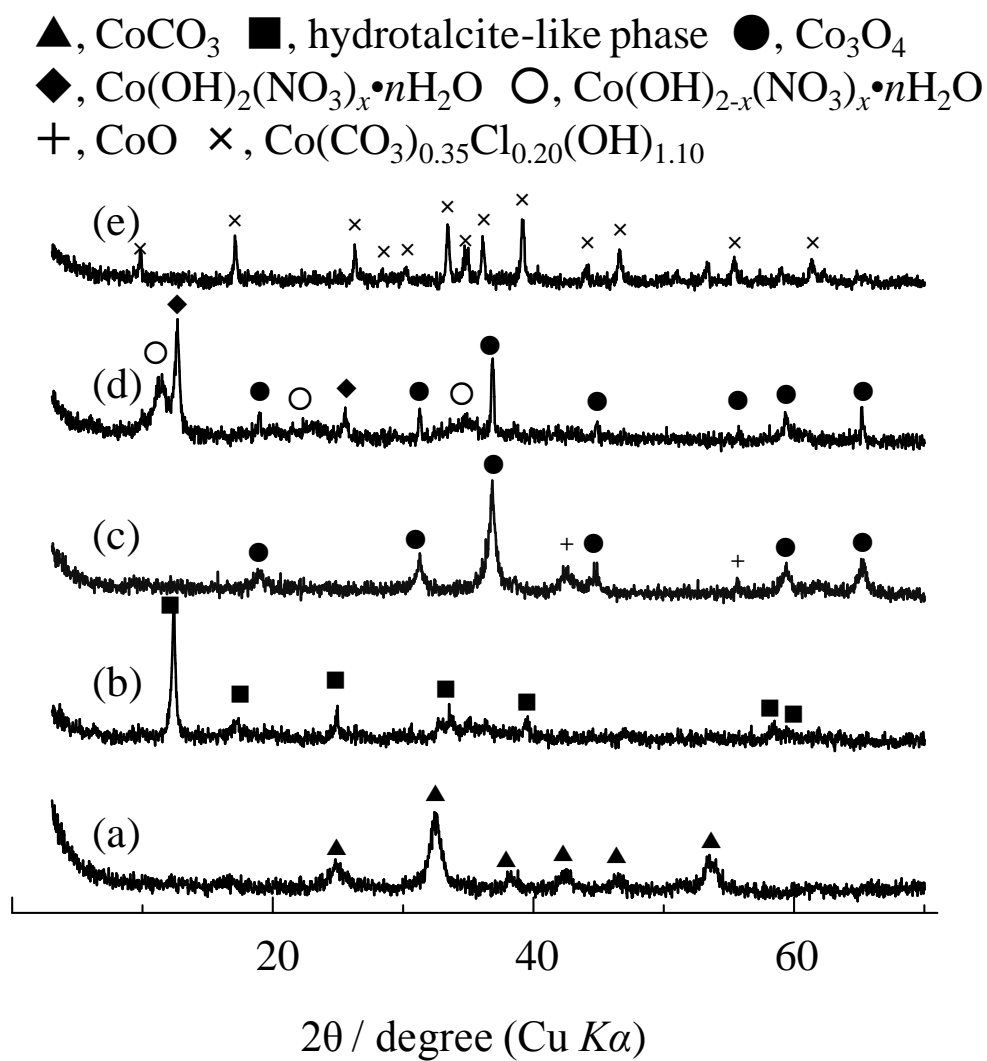
Catalyst	Co salt source	Synthesis method	Precursor phase
A	cobalt(II) carbonate	impregnation	CoCO_3
A'	cobalt(II,III) oxide	impregnation	Co_3O_4
B	cobalt nitrate hexahydrate	homogeneous precipitation	hydrotalcite-lile
C	cobalt nitrate hexahydrate	combustion with glycine	Co_3O_4 , CoO
D	cobalt nitrate hexahydrate	gradual oxidation	Co_3O_4 , $\text{Co}(\text{OH})_2(\text{NO}_3)_x \cdot n\text{H}_2\text{O}$, $\text{Co}(\text{OH})_{2-x}(\text{NO}_3)_x \cdot n\text{H}_2\text{O}$
E	cobalt chloride hexahydrate	hydrothermal	$\text{Co}(\text{CO}_3)_{0.35}\text{Cl}_{0.20}(\text{OH})_{1.10}$

Table 2 Crystallite sizes and BET surface areas of K-doped Co₃O₄ catalysts

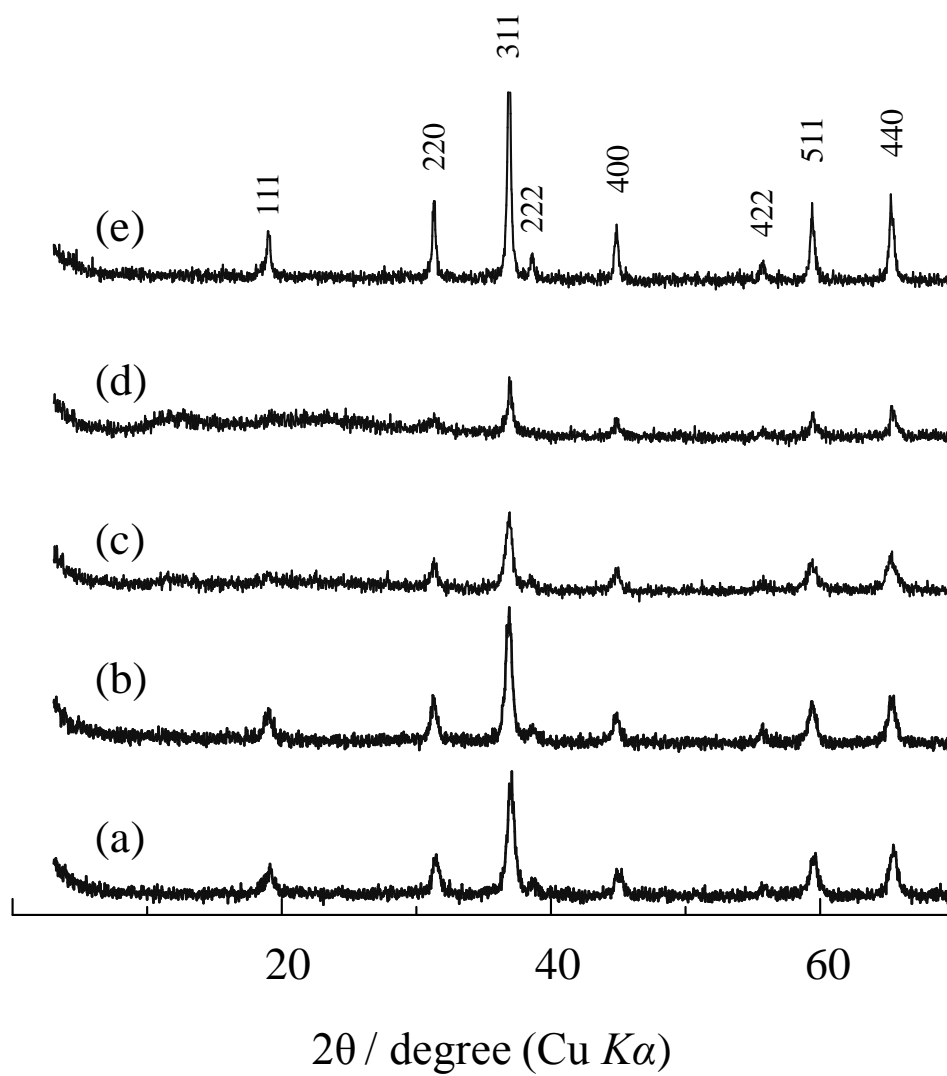
Catalyst	Fresh catalyst		Sent catalyst	
	Crystallite size (nm)	BET surface area (m ² /g)	Crystallite size (nm)	BET surface area (m ² /g)
A	22	56	25	36
B	25	39	20	29
C	21	14	31	14
D	56	27	63	24
E	55	18	63	15

Table 3 XPS results for the catalysts

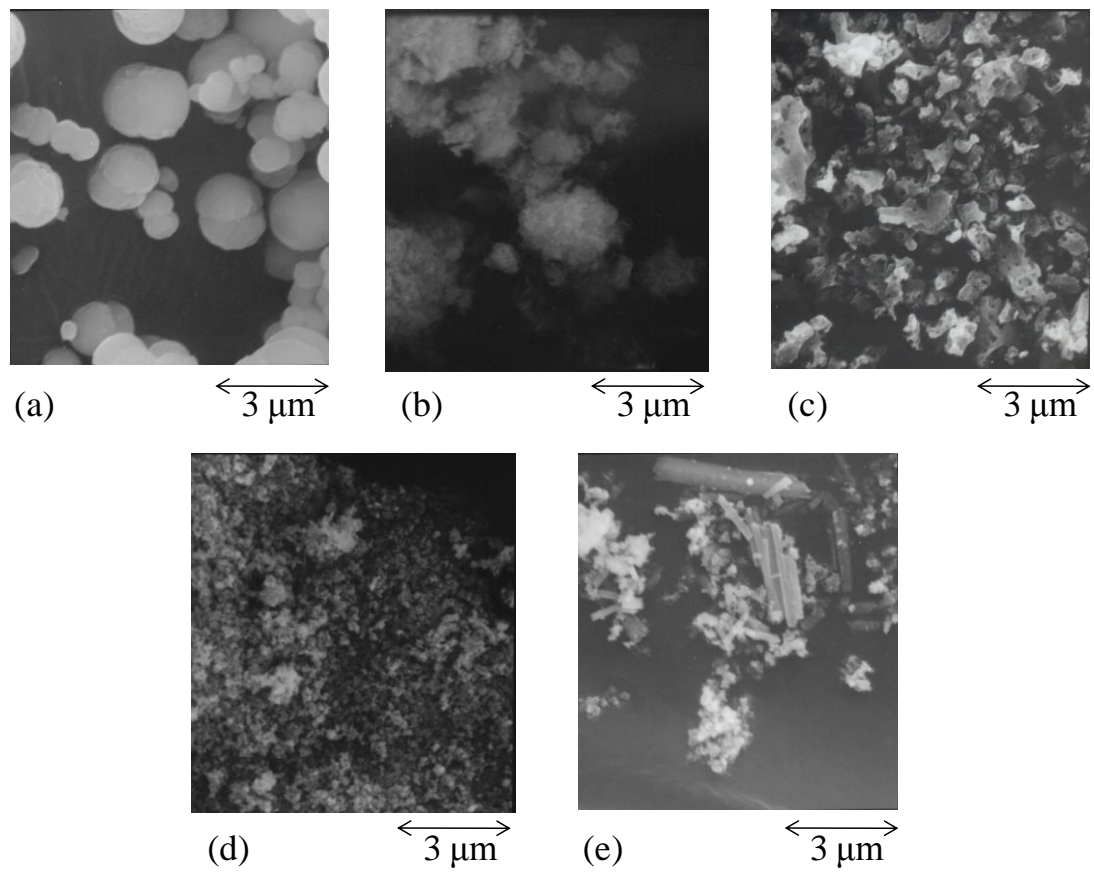
Catalyst	Co 2p _{3/2} Binding energy (eV)	Surface composition		
		K/Co	Other element (X) detected	X/Co
A	779.7	0.116	—	—
B	780.0	0.077	—	—
C	779.6	0.108	—	—
D	779.8	0.059	Na	0.493
E	780.1	0.039	Cl	0.071



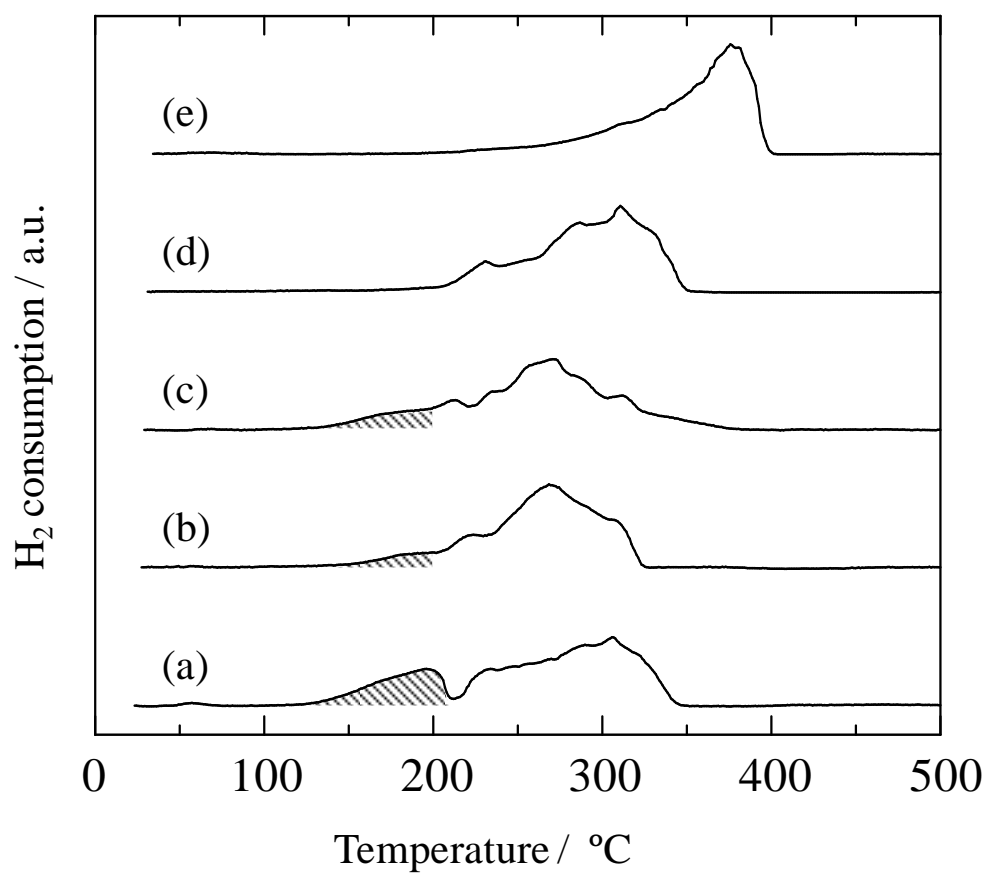
Yoshino et al., Figure 1



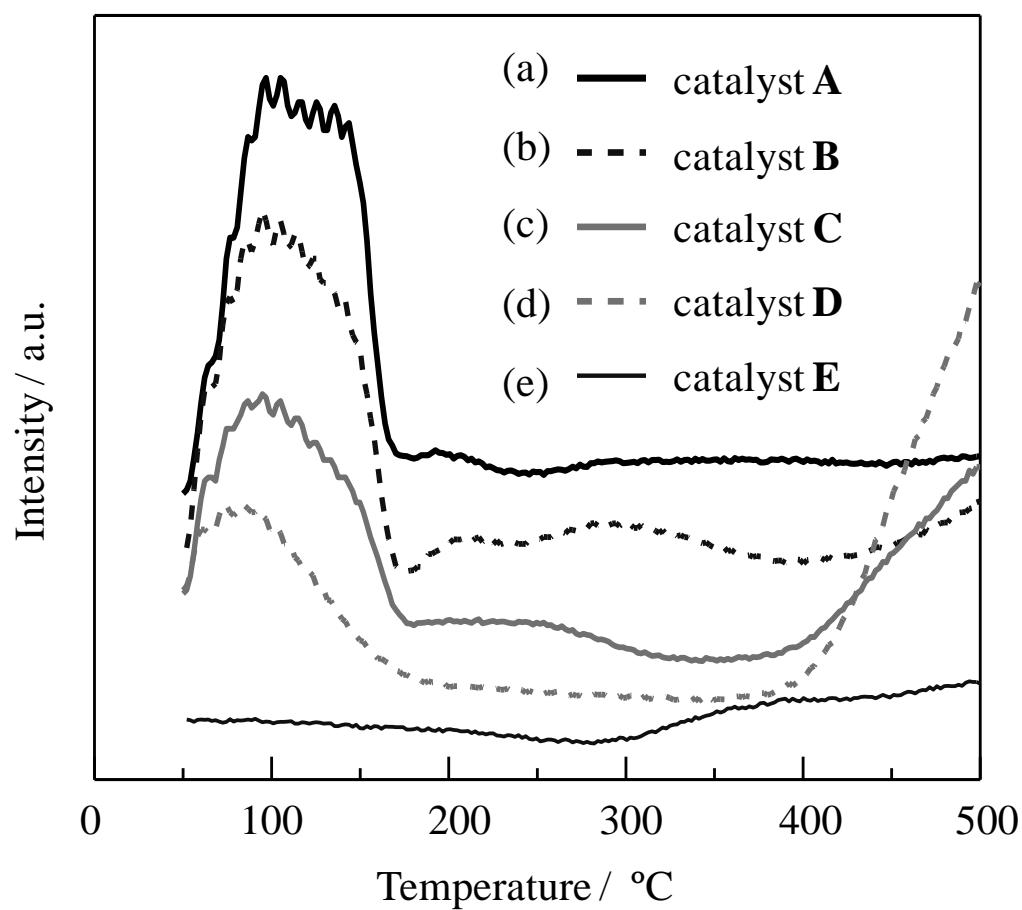
Yoshino et al., Figure 2



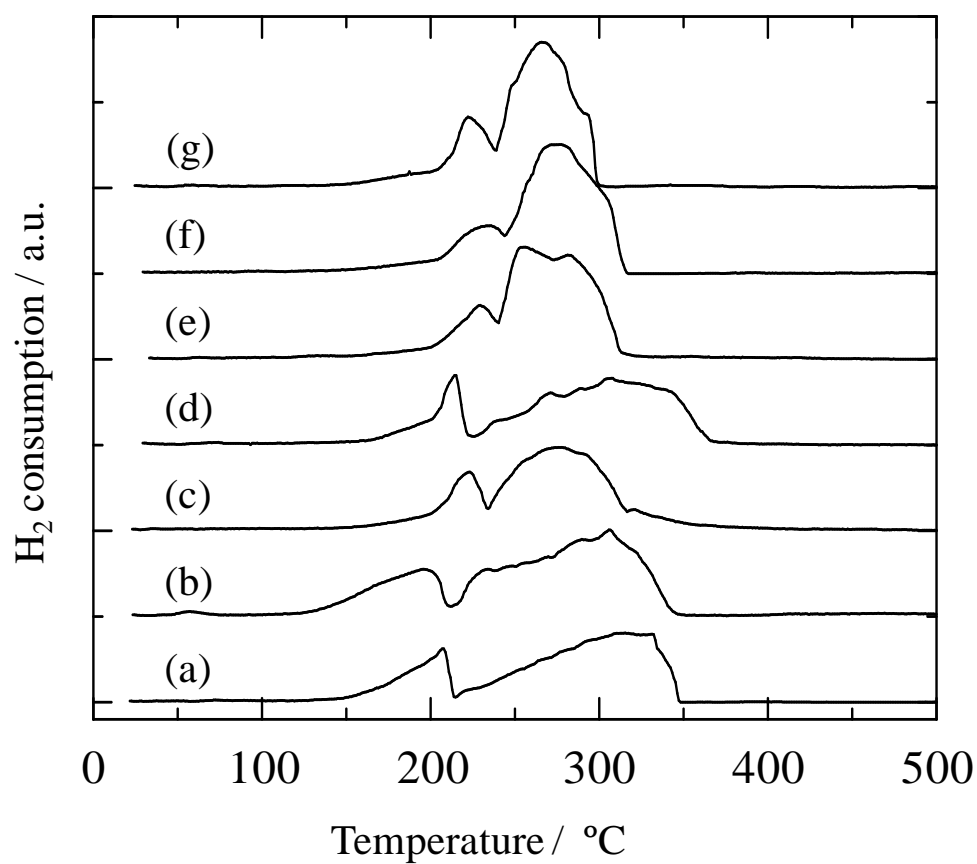
Yoshino et al., Figure 3



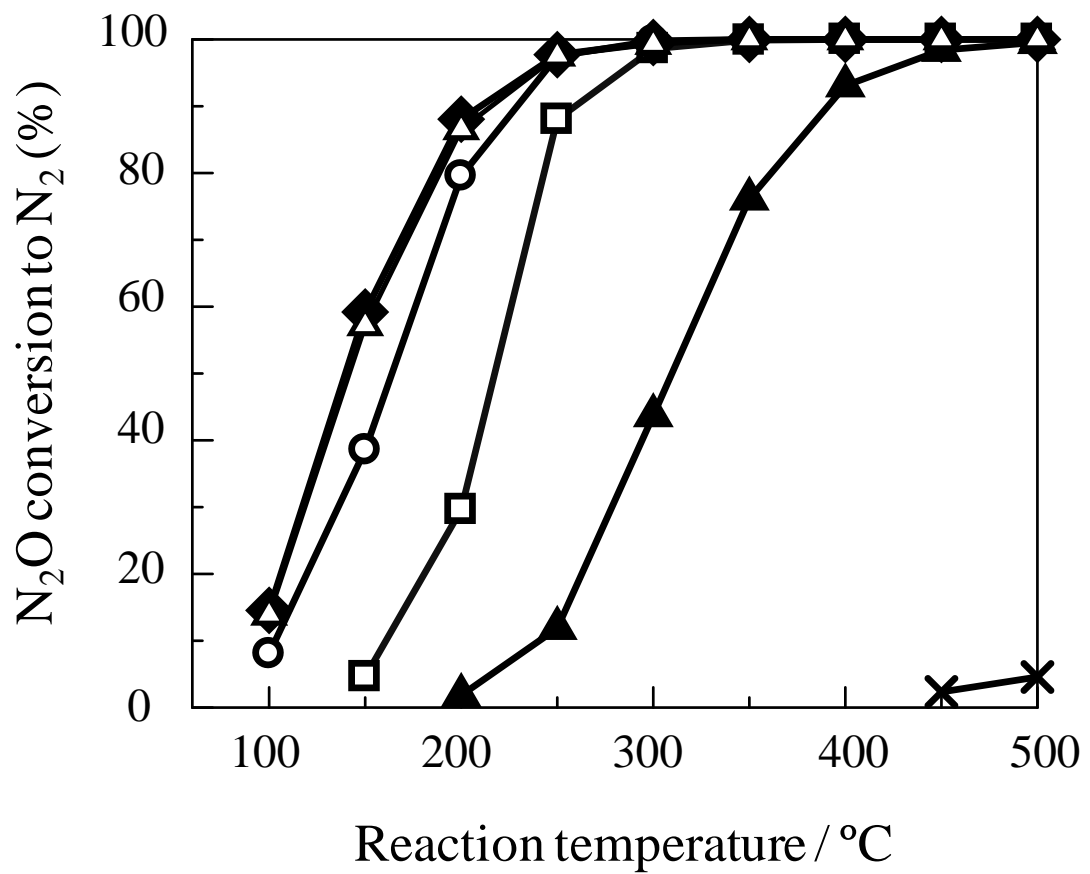
Yoshino et al., Figure 4



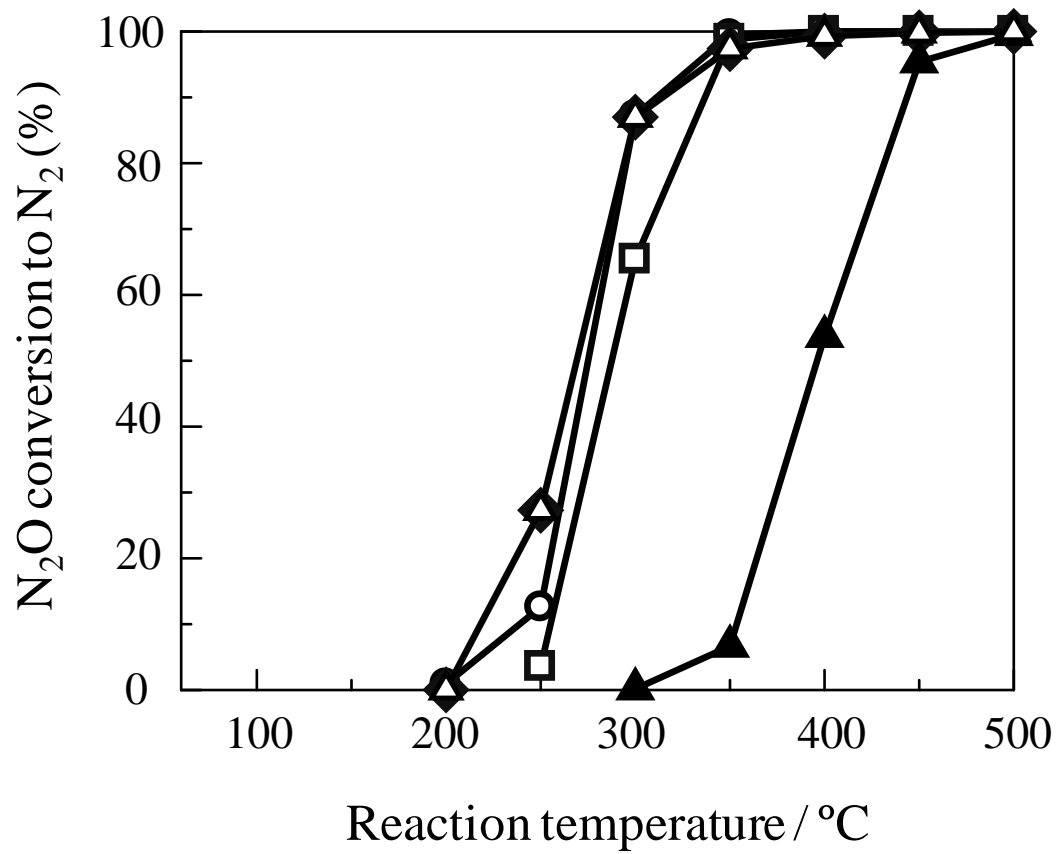
Yoshino et al., Figure 5



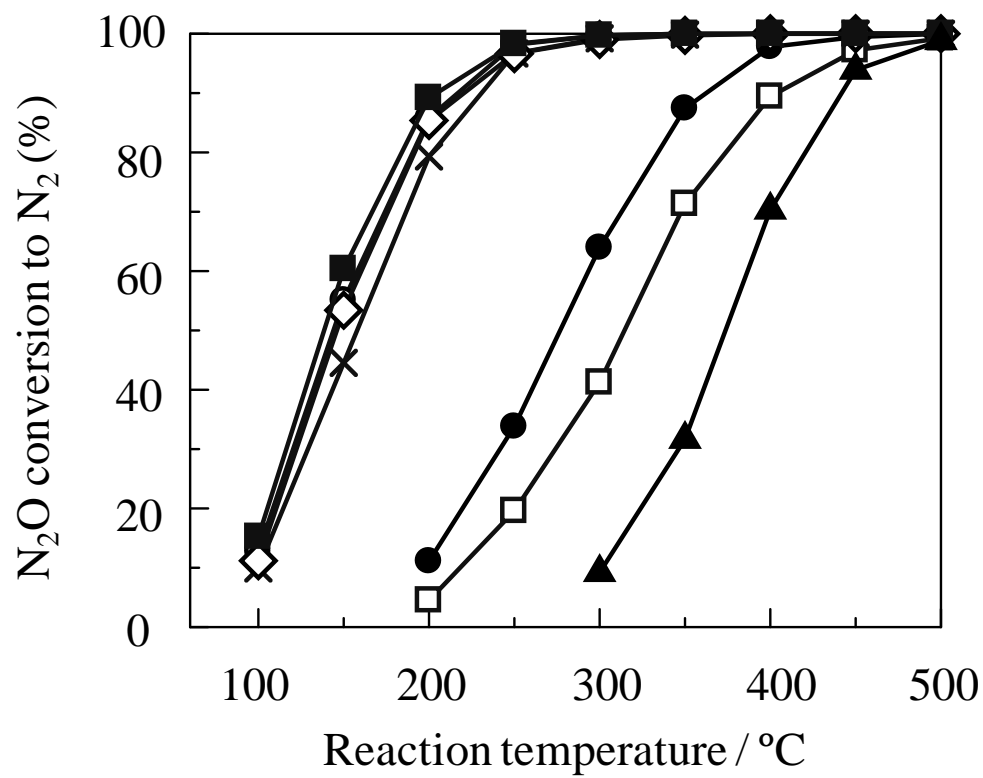
Yoshino et al., Figure 6



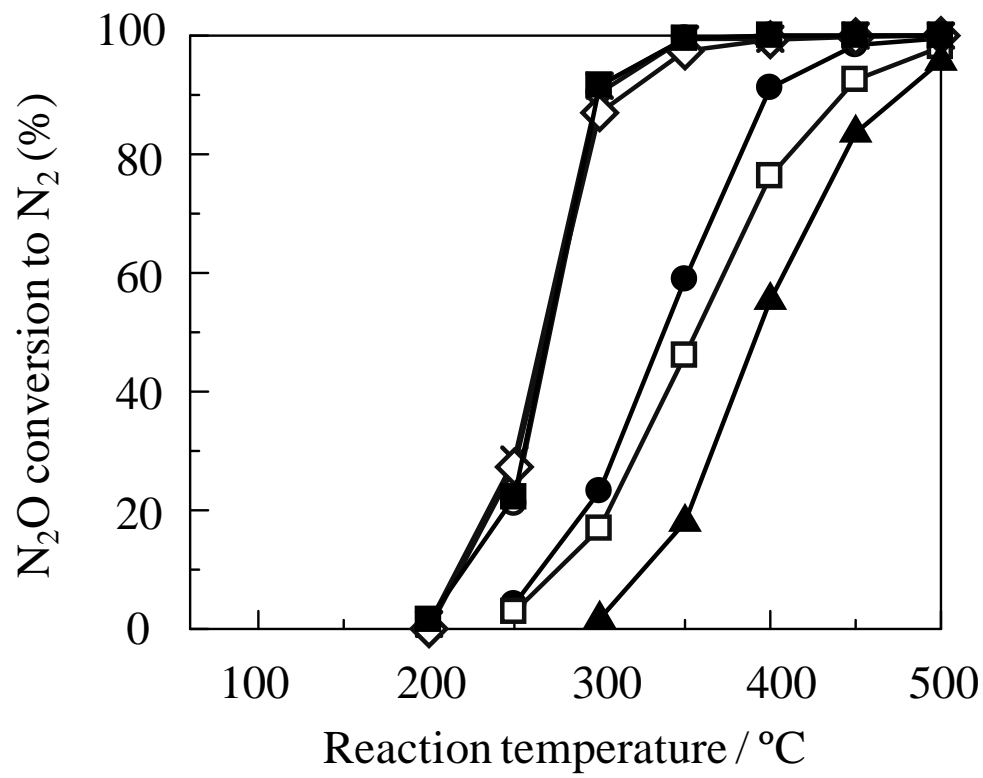
Yoshino et al., Figure 7



Yoshino et al., Figure 8



Yoshino et al., Figure 9



Yoshino et al., Figure 10